Optical Measurement of Conduction in Single Demyelinated Axons

Peter Shrager and Chaim T. Rubinstein

From the Department of Physiology, University of Rochester Medical Center, Rochester, New York 14642

ABSTRACT   Demyelination was initiated in *Xenopus* sciatic nerves by an intraneural injection of lysolecithin over a 2–3-mm region. During the next week macrophages and Schwann cells removed all remaining damaged myelin by phagocytosis. Proliferating Schwann cells then began to remyelinate the axons, with the first few lamellae appearing 13 d after surgery. Action potentials were recorded optically through the use of a potential-sensitive dye. Signals could be detected both at normal nodes of Ranvier and within demyelinated segments. Before remyelination, conduction through the lesion occurred in only a small fraction of the fibers. However, in these particular cases we could demonstrate continuous (nonsaltatory) conduction at very low velocities over long (greater than one internode) lengths of demyelinated axons. We have previously found through loose patch clamp experiments that the internodal axolemma contains voltage-dependent Na^+ channels at a density ~4% of that at the nodes. These channels alone, however, are insufficient for successful conduction past the transition point between myelinated and demyelinated regions. Small improvements in the passive cable properties of the axon, adequate for propagation at this site, can be realized through the close apposition of macrophages and Schwann cells. As the initial lamellae of myelin appear, the probability of success at the transition zone increases rapidly, though the conduction velocity through the demyelinated segment is not appreciably changed. A detailed computational model is used to test the relative roles of the internodal Na^+ channels and the new extracellular layer. The results suggest a possible mechanism that may contribute to the spontaneous recovery of function often seen in demyelinating disease.

INTRODUCTION

When axons are demyelinated, conduction is at first blocked, but later often recovers even in the absence of remyelination. Bostock and Sears (1978) measured longitudinal currents from axons within intact ventral roots and found that inward currents appeared in internodal regions after demyelination. They suggested that Na^+ channels, thought normally to be confined to nodes (Ritchie and Rogart, 1977), may migrate or be synthesized in response to the myelin removal. They noted, however, that computational models (Koles and Rasminsky, 1972) predicted that

improvements in passive cable properties of the fiber should also be necessary for successful conduction. More recently, we measured ionic currents at paranodal and internodal sites in single demyelinated amphibian and mammalian fibers using a loose patch clamp technique (Shrager, 1987, 1988, 1989). We showed that the internodal axolemma had a Na^+ channel density of ~4% of that at the nodes, and that this was constant from 1 d to several months after the initiation of demyelination, suggesting that these channels were present in the normal cell as well. A sharp gradient in density of Na^+ channels existed at the nodes of Ranvier, and this persisted throughout the period of demyelination and remyelination, suggesting that lateral diffusion must be limited to just a fraction of the nodal channels. We were also able to demonstrate that propagating action potentials invading a demyelinated region were capable of activating the internodal Na^+ channels under some conditions (Shrager, 1988). Because of the very large difference in length, despite their much lower density, the total number of internodal Na^+ channels is ~40 times the total number of nodal channels (Shrager, 1987; Chiu and Schwarz, 1987). These channels should not be activated during normal conduction. The question that remains is whether they play any effective role in conduction after myelin removal. If demyelinated internodes conduct as unmyelinated fibers, then propagation should proceed in this region at constant velocity. Calculations from the computational model presented below predict that, with a Na^+ channel density of 4% of the nodal value, this velocity should be ~1 m/s. If the internodal Na^+ channels are present at all times, why is conduction blocked, and what events are responsible for its restoration?

In order to investigate this problem, we needed a technique that would allow us to follow action potentials along a fiber whose structure varies markedly over sharp boundaries, and we thus required good spatial resolution. Optical recording, using potential-sensitive dyes, is a method that has been refined significantly over the past several years (Cohen and Salzberg, 1978; Grinvald, 1985; Cohen and Lesher, 1986). Signals have been obtained from demyelinated nerve bundles (Lev-Ram and Grinvald, 1986, 1987; Shrager et al., 1987) and it is now possible to record from very fine processes of neurons (Grinvald et al., 1981). We thus sought to use this system to measure action potentials from single intact nodes of Ranvier, as well as from defined sites on demyelinated internodes. In this paper we investigate conduction in demyelinated axons and emphasize the critical period of time when conduction just begins to recover. We characterize axonal ultrastructure in detail and correlate this with changes in the pattern of excitation. The results suggest that conduction failure may be reversed by very small changes in the extracellular barrier at critical sites, a result that may be relevant in functional changes in demyelinating disease.

A brief preliminary account of this work has been published (Shrager et al., 1989; Rubinstein and Shrager, 1989).

METHODS

Axon Preparation and Demyelination

Frog nerves were demyelinated using lysolecithin, a technique developed originally in the mouse by Hall and Gregson (1971). *Xenopus* were anesthetized in tricaine methanesulfonate (3.7 g/liter H_2O) and the sciatic nerve in one leg was surgically exposed. 1 μl of sterile frog

Ringer's solution containing 1% lysolecithin was injected into both tibial and peroneal branches in the thigh using a glass micropipette broken to a tip diameter of 18–20 μm. The wound was sutured and the animal was allowed to recover. On the day of the experiment the frog was anesthetized in ice water and killed by decapitation. The injected nerve was dissected and desheathed and sealed with Vaseline in a chamber fitted with pairs of platinum wires for electrical stimulation and recording. The preparation was soaked in a solution of frog Ringer's containing collagenase (3.5 mg/ml) and the dye RH155 (Lev-Ram and Grinvald, 1986; available as NK 3041, from Nippon Kankoh-Shikiso Kenkyusho, Okayama, Japan), 1–2 mg/ml, for 1.5–2 h. The solution was then changed to frog Ringer's alone. Optical recording began ~15 min after removal of the dye. Compound action potentials measured after this treatment had patterns of conduction times of normal and remyelinating fibers that were similar to those reported earlier in loose patch clamp experiments with no dye exposure (Shrager, 1988). The nerve was then dissociated into individual axons by very gentle mechanical spreading, with the outermost fibers held in place with Vaseline. The dissection and spreading procedures used were identical to those employed for loose patch clamp experiments and further details are given there (Shrager, 1987, 1988). The preparation was typically restained for 10–15 min after 1.5–2 h of recording. In earlier work on whole, desheathed sciatic nerves (Shrager et al., 1987) some other dyes were tested (RH42, RH479, and RGA333) but RH155 gave the largest signal-to-noise ratio. Immediately after the experiment the nerve was fixed for electron microscopy according to procedures described in detail previously (Shrager, 1988).

The Ringer's solution contained (in millimolar): NaCl 115, KCl 2.5, $CaCl_2$ 1.8, HEPES 5, pH 7.4. All experiments were run at room temperature.

Optical Measurements

A microscope (Diaphot, Nikon, Inc., Garden City, NY) was modified primarily to improve the source of illumination. Light from a 50-W tungsten-halogen lamp (Philips Electronic Instruments, Inc., Mahwah, NJ) backed by a spherical mirror was collected by a condenser (Oriel Corp., Stratford, CT) and collimated by a 300-mm tube lens (Melles Griot, Rochester, NY). The beam was passed through an interference filter (705 ± 25 nm bandwidth, Omega Optical, Inc., Brattleboro, VT) and a rectangular variable aperture (E. Leitz, Inc., Rockleigh, NJ) and was then focussed with a 0.65 N.A. condenser (Nikon, Inc.). An electronic shutter (Vincent Associates, Rochester, NY) served to limit the time of exposure. An image formed by a ×40, ×20, or ×10 objective was projected on to one element of a linear array of photodiodes (LD12-5-A, Centronic, Mountainside, NJ) via a lens connected to the side port of the microscope (Amarel Precision, Penfield, NY). Except where noted, all records were made with the ×40 objective, for which the photodiode covered an image field corresponding to a 10 × 10-μm square. The microscope was insulated from noise due to mechanical vibration by two stages of inflated rubber doughnuts (Newport Corp., Fountain Valley, CA).

The photodiode served as input to a current-to-voltage converter with variable gain and a time constant of 50 μs. A laboratory computer controlled the illumination, generated stimuli, and digitized and stored the data. Optical signals were passed through a programmable eight-pole Bessel filter (Frequency Devices, Haverhill, MA), usually set to 1–3 kHz, before sampling at 12.5–25 kHz. In general, 64 sweeps were averaged for each record, stimulating at 10 Hz. The stimulating pulses were synchronized to the sampling clock to prevent the introduction of jitter that could distort the averaged data. Some asynchrony could in principle occur with small changes in conduction times with successive sweeps. However, when the compound action potential was passed through the data channel normally used for optical signals, the result of averaging 8 or 64 sweeps was indistinguishable from that with just a single sweep, indicating that any distortion from this source is negligible. Optical signals are expressed as the fractional change in transmitted light intensity. During analysis the data were usually dig-

itally filtered using a Gaussian routine (Colquhoun and Sigworth, 1983). The overall cutoff frequency (F_c) was calculated from the electronic and software filtering steps (Colquhoun and Sigworth, 1983) and is given for each record. Peak values and the time to 50% peak were determined by fitting the relevant portions of the curves with a 3rd order polynomial (Hille, 1971). After spreading, the axons formed a two-dimensional network. Averaged over large distances the axons were essentially parallel. However, on a smaller scale they crisscrossed at several points. To insure that signals originated from the axon under study two precautions were taken. Records were made at several widely spaced sites along a fiber, so that interference from scattered light from a crossing axon would not be seen beyond one site, and further, the photodetector was often centered at sites two to three axon diameters to either side of the axon and the measurement was repeated. If signals did not fall off rapidly with radial distance, they were deemed to result from crossing fibers and the data were discarded. It is possible, however, that in some cases a small portion of the recorded signal results from scattered light from a nearby cell. After dissociation, small bundles of axons with a very uniform morphology were sometimes seen. These probably resulted from a channeling of the lysolecithin within the cord during injection. Recordings were made along the center of these tracts, which consisted typically of five to eight fibers.

Computational Model

A model for calculating action potentials in demyelinated axons was built around the EXTCABLE numerical integration system developed by Drs. M. Hines and J. W. Moore, Department of Neurobiology, Duke University, Durham, NC (Hines, 1989). We are grateful to Drs. Moore and Hines for their hospitality during a visit to Duke, and for modifying the program to include Xenopus channels and the capability to alter the circuit representing the extracellular layer. We wrote the present scheme using the FOCAL interpreter, which set up the cable geometry, passive properties, and channels, and controlled the integration through subroutine calls to EXTCABLE. The model axon consisted of 12 nodes and 11 internodes, with the demyelination occurring in the central internode, as shown in the sketch at the top of Fig. 1. The cable segments were numbered as illustrated. The demyelinated internode was divided into 20 segments of equal length. The passive elements in the electrical equivalent circuit utilized are shown in the lower diagram in Fig. 1. G_m and C_m refer to the axolemma, and G_x and C_x apply to the extracellular layer. R_i represents the axoplasm resistance and R_{FH} is the axial resistance in the Frankenhaeuser-Hodgkin (1956) space between the axolemma and the extracellular layer. The equations describing the voltage-dependent Na^+, K^+, and P^+ channels added to the axolemma were those determined by Frankenhaeuser and Huxley (1964) for Xenopus. The passive and voltage-dependent properties of each segment of normal and demyelinated axon could be individually specified. The values that were constant for all simulations are given in Table I. Numerical integration was usually carried out for 10 ms with a time step of 0.05 ms. When necessary for a comparison with the optical records the resulting computed signals were digitally filtered with the same Gaussian routine as used above, and with an F_c equal to that of the experimental data.

RESULTS

Ultrastructure of Demyelinated and Remyelinating Axons

After the intraneural injection of lysolecithin, myelin is rapidly damaged, with altered morphology and debris-covered breaks appearing within <1 d (Hall and Gregson, 1971; Shrager, 1987). Macrophages then appear within the lesion, increasing in number over the first week after surgery, and remove all of the damaged myelin within the lesion by phagocytosis. Beginning at ~1 wk after the initial

demyelinating event proliferating Schwann cells are also apparent throughout the lesion and these may be seen to attach to the newly bared axolemma, ultimately resulting in remyelination. We have previously described much of this progression through electron micrographs covering a wide time frame (Shrager, 1987, 1988). The pictures in Fig. 2 emphasize the events occurring during the critical period
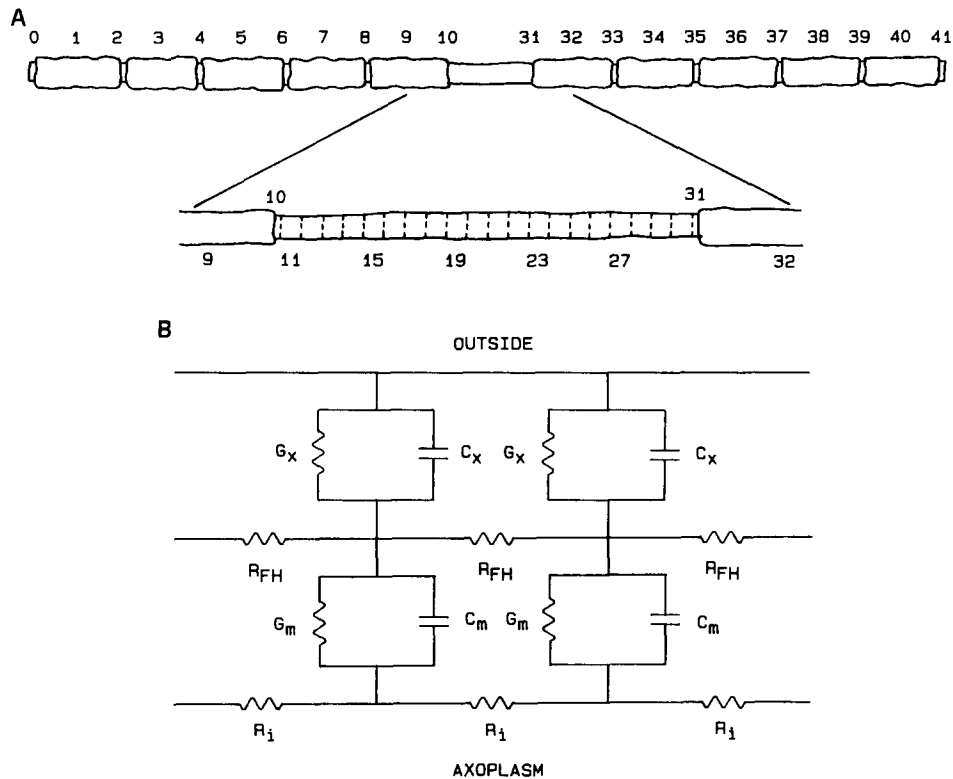

FIGURE 1. Modeling conduction in demyelinated axons. (A) A schematic drawing of the fiber, showing the numbering of nodes and internodes. The central internode was divided into 20 segments of equal length, numbered 11 through 30. Segments 10 and 31 represent the nodal membrane bordering this demyelinated zone. (B) The electrical equivalent circuit used in the calculations. Two segments and their interconnecting components are illustrated. All components can be individually stipulated for each segment. G_x and C_x represent the myelin or Schwann cell extracellular layer. R_{FH} is the axial resistance of the Frankenhauser-Hodgkin (1956) space containing extracellular fluid between the Schwann cell/myelin layer and the axolemma. G_m and C_m represent the leakage conductance and the capacitance of the axolemma. The voltage-dependent channels which are in parallel with these are not shown in this diagram. R_i is the axoplasmic resistance.

during which conduction is first restored. In Fig. 2 *A* a macrophage is removing the last remaining remnants of myelin from an axon, 8 d after injection. Note the large quantity of myelin debris already ingested by the macrophage. Fig. 2 *B* shows at higher magnification the close apposition between a macrophage (*left*) and the axolemma. Between 8 and 11 d Schwann cells can be seen adhering to demyelinated

axons, and by 12–13 d the first few lamellae of new myelin appear (Fig. 2 C). Remyelination continues to progress over the next several days, though the new myelin is not yet fully compact (Fig. 2 D).

As a means of obtaining a quantitative view of the progress of remyelination we visually scanned several sections in the electron microscope and divided the axons into several categories. The histograms in Fig. 3 A show the results. The label N on the abscissa denotes naked axons. P represents fibers with <100% of their surfaces covered by attached Schwann cell processes. The numbers on the abscissa give the number of turns of Schwann cell and myelin present (1 denoting just one complete turn of the Schwann cell). A total of 177 cells were examined. There is a fairly smooth progression over the 6 d studied. The fraction of bare fibers declines, with the first few turns of myelin appearing at 12 d after injection. Thus, before this

TABLE I

Parameters of Conduction

Parameter	Location	Value	Unit
P_{Na}	Nodes	0.008	cm/s
P_K	Nodes	0.0012	cm/s
P_p	Nodes	0.00054	cm/s
G_m	Nodes	0.0303	S/cm^2
G_m	Internodes	0.0005	S/cm^2
C_m	Nodes	2	$\mu F/cm^2$
C_m	Internodes	1	$\mu F/cm^2$
V_{rest}	All	−65	mV
G_x	One myelin membrane	0.0004	S/cm^2
C_x	One myelin membrane	1	$\mu F/cm^2$
R_{FH}	Normal nodes	10^6	$M\Omega$

R_{FH} joining demyelinated segments that are covered by a cellular layer is calculated using a resistivity of Ringer's solution of 80 Ω-cm (Milton et al., 1985). R_i joining all segments is calculated using an axoplasmic resistivity of 110 Ω-cm (Stampfli, 1952). Values for nodal channel maximum permeabilities, G_m, and C_m are from Frankenhaeuser and Huxley (1964). The number of myelin lamellae covering normal internodes was set to 75–125, depending on the axon diameter, as measured in micrographs. The resting potential was set to −65 mV, since on voltage clamp simulation this resulted in a resting inactivation of ~50% with variations in holding potential, similar to the value obtained in loose patch clamp experiments on demyelinated axons (Shrager, 1987, 1988).

time, conduction through a demyelinated zone must occur without the aid of myelination. These results are summarized in the graph of Fig 3 B where we plot the percentage of axons with more than one Schwann cell lamella vs. time postsurgery.

A profile of successful conduction through the lesioned zone can be obtained from compound action potentials. A series of these records covering in detail the days during which Schwann cells first appear and then develop the initial new lamellae of myelin is shown in Fig. 4. In A sweeps are plotted at different gains in order to magnify the very small signals at early times. In B all records are at the same gain to emphasize differences in amplitudes. In general, the injected lysolecithin demyelinates >90% of the fibers in each branch, but leaves a small number with a normal

appearance under light microscopy. Correspondingly, in most compound action potential records there is a small component with a fast conduction velocity that represents these axons. This peak is indicated with an arrow in several sweeps of Fig. 4. All other components represent demyelinated or remyelinating fibers. Before the appearance of proliferating Schwann cells (6–8 d) conduction through most axons is blocked. There is a wide spectrum of propagation times represented, but only a small fraction of the axons are conducting successfully through the lesion (note scales at left). Since the injected zone occupies only the central 2–3 mm out of the 14 mm between stimulating and recording wires, the slowing of conduction in this zone is actually much more marked than appears in the figure. Over the time studied the conduction velocity improves by a factor of 2–3, whereas the amplitude of the slow signals increases about 15-fold.

Optical Recording of Conduction

Optical records of action potentials from single normal nodes of Ranvier are shown in Fig. 5 *A*. The records represent the fractional change in transmitted light in two successive nodes in an axon from an uninjected nerve. From the difference in 50% rise times we calculate a conduction velocity through this internode of 15 m/s. In this and succeeding figures we show a schematic diagram of the axon, with p indicating the proximal end and d the distal end. Stimulation was applied to the proximal end of the nerve. In Fig. 5 *B* we illustrate signals at short spacing about a node. At the top the photodiode field was centered 11 μm proximal to a normal node. Successive traces were centered on the node, 11 μm distal to the node, and much further into the internode. The signal-to-noise ratio at the paranodes is insufficient for a comparison of the time course with that of the nodal records. It is likely that the small signals recorded at the paranodes originated at the nodal axolemma and reached the photodiode through light scattering. The paranodal axolemma would be well insulated by myelin if the paranodal seals were tight. Furthermore, the paranodal membranes were probably not readily accessible to the dye. Although stain was visible in this region, the resting light intensity was not measurably different from that at the node despite the fact that there were perhaps 250 times the number of membranes in the field (the effective factor is actually closer to 750 since the nodal membrane occupied ~20% of the photodiode field, while the paranode occupied ~60%). The spatial resolution along the axon is thus about one axon diameter for well-isolated fibers. With less spreading, scattering was more severe, and limited the spatial resolution to about 50 μm.

Fig. 5 *C* shows calculated action potentials from two successive nodes in a model axon with dimensions similar to those of the axon of Fig. 5 *A*. The calculated action potentials are of somewhat shorter duration than the optical signals, but are otherwise quite similar. The model conduction velocity in this case was 19 m/s, close to the experimentally determined value. In Fig. 5 *D* the internodal Na^+ channel density was set to zero. The calculated spikes and velocity were unchanged, as would be expected if the internodal Na^+ channels played no role in conduction in normal myelinated axons.

At 8 d after injection axons are completely demyelinated and conduction across the lesion is rare. Newly bound Schwann cells are few in number, but macrophages
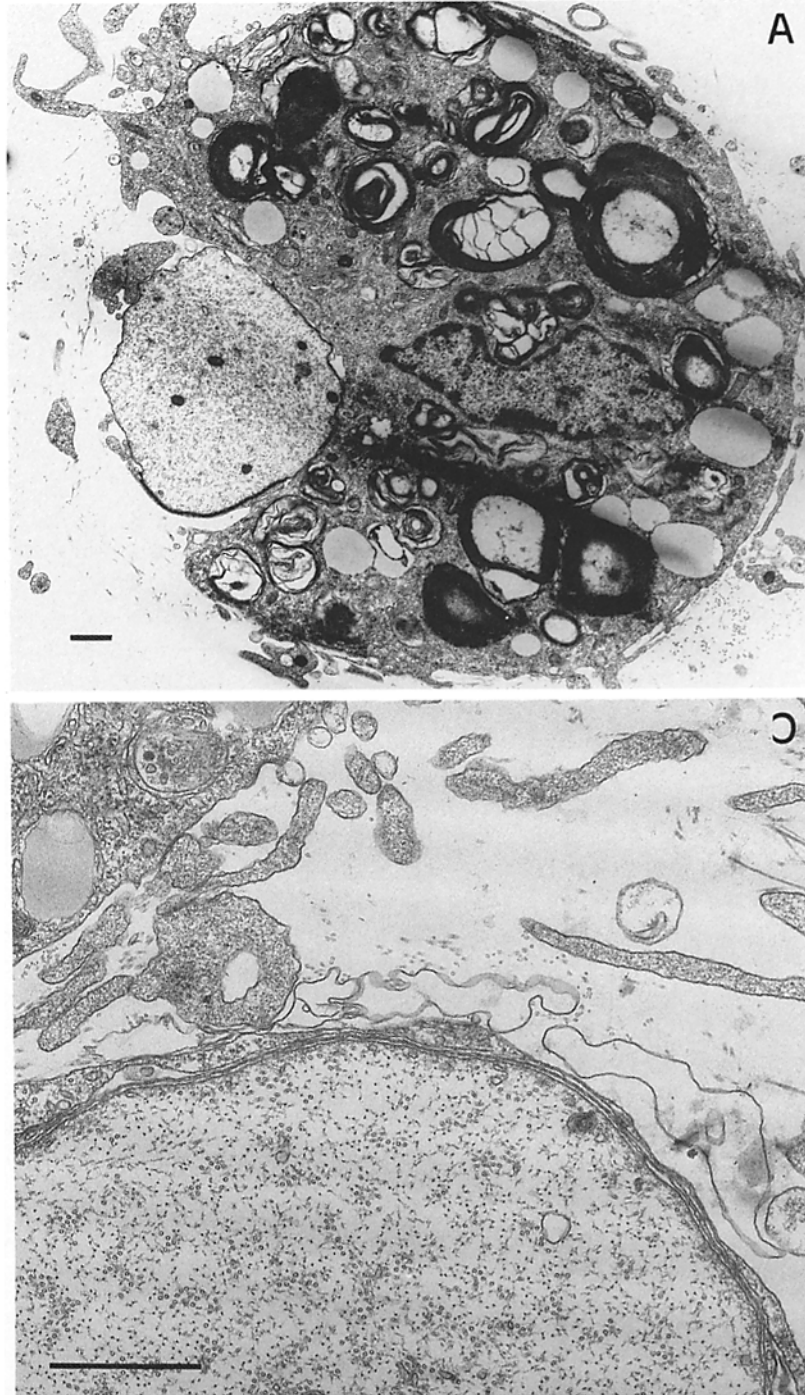
FIGURE 2. Electron micrographs of thin sections of axons and associated cells. (A) A macrophage (*left*) removing damaged myelin from an axon, 8 d after injection. (B) A macrophage (*left*) and axon at higher magnification, showing the close association of the two cells, 8 d after surgery. (C) An remyelinating axon with two turns of the Schwann cell, 13 d after injection. (D) Further remyelination, 15 d after surgery. (*Inset*) The new, uncompacted myelin at higher magnification. Bars, 1 μm, except in inset to D, which is 0.25 μm.
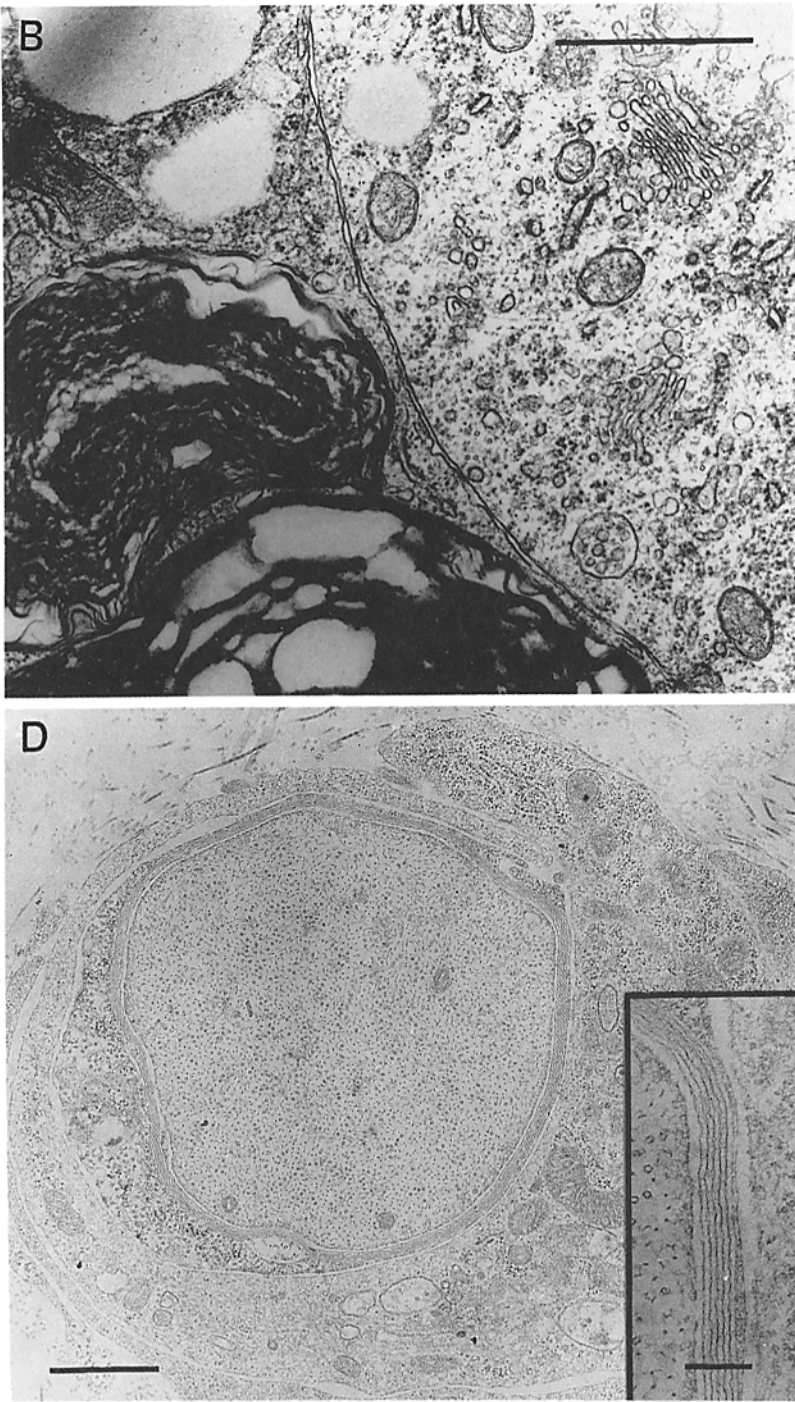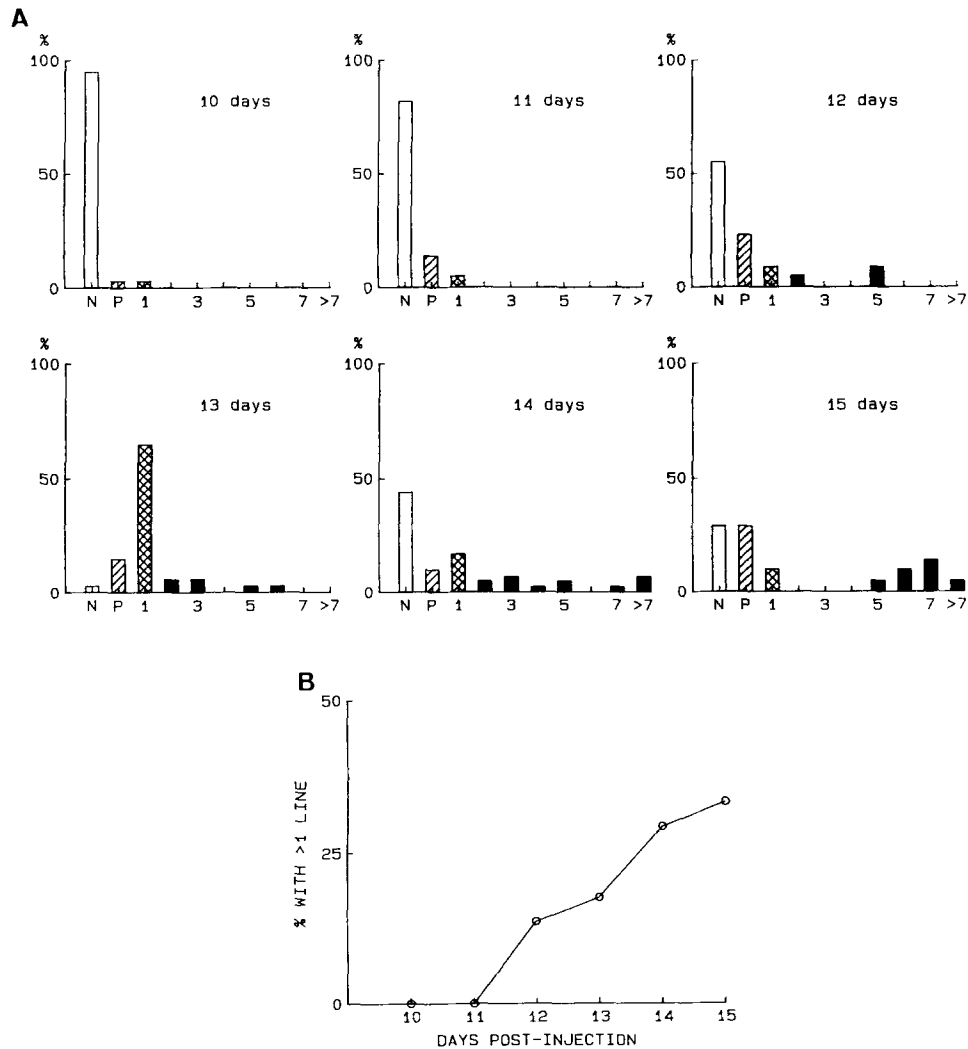
FIGURE 2. (*continued*)

A

B

FIGURE 3.   The time course of remyelination. (A) Histograms illustrating the development of remyelination 10–15 d after injection. The abcissa shows the degree of remyelination. N, naked axons. P, axons with Schwann cell processes, but with less than one complete turn of the Schwann cell. The numbers give the number of turns of Schwann cell and myelin. The ordinate plots the percentage of cells in each state. A total of 177 cells were counted. (B) A plot of the percentage of cells with more than one lamella vs. the number of days after injection.

frequently remain attached to the axon at several points. There is in general a sharp transition from normal-looking myelin to bare axon often, but not always, at a former node of Ranvier (judged by the internodal distance common for a given diameter fiber). Optical studies demonstrate that conduction failure typically occurs abruptly at this transition point. An example is shown in Fig. 6 A. An action poten-

tial was recorded at the node of Ranvier 1.7 mm proximal to the demyelinated zone, but no signal could be detected at or beyond the end of myelin. In this case macrophages were found attached to the axolemma, but with only a very sparse distribution in the initial segment of the demyelinated region (Fig. 6 C). A model of this axon produces the same result (Fig. 6 B). The sparse macrophage covering was modeled as a single-cell (two-membrane) layer covering segments 12, 14, 18, 22, 26, and 29, spaced 200 Å from the axolemma, which was the average value measured
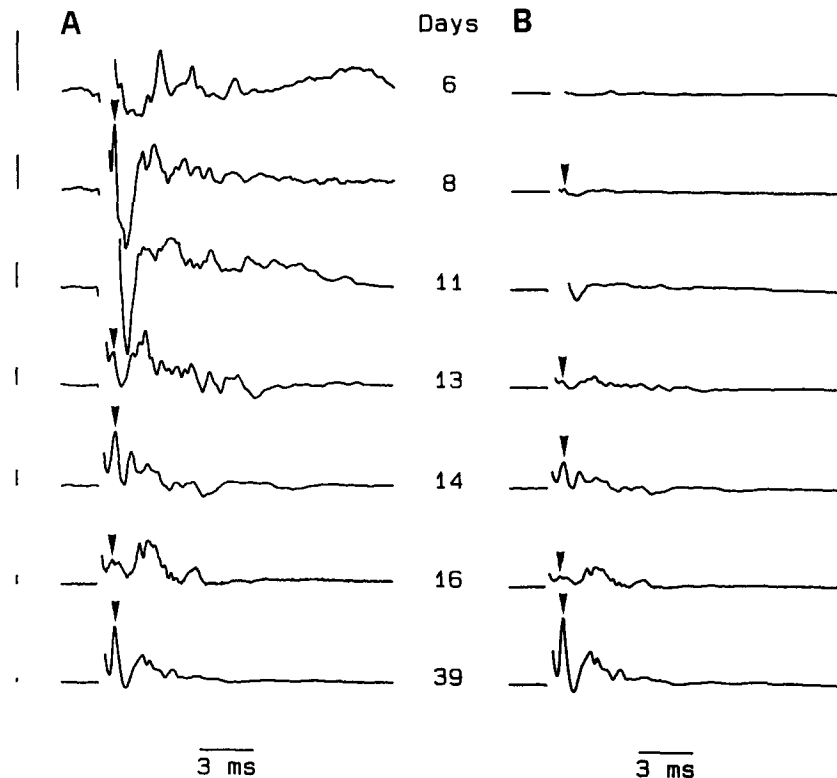

FIGURE 4. Compound action potentials recorded from demyelinated nerves. The numbers in the central column give the days after surgery. Arrows point to components reflecting fibers that were not demyelinated by the lysolecithin injection (see text). In *A* the scale bar at the left of each trace represents 5 μV at the recording electrodes. In *B* all sweeps are plotted at the same gain. The stimulus artifact has been blanked from the records. The distance between stimulating and recording electrodes was 14.5 mm.

from electron micrographs. The axial resistance (R_{FH}) was calculated for a layer of extracellular fluid of this thickness and the covering was therefore "loose"; i.e., no tight seals were included. Despite the presence of internodal Na^+ channels at a density 4% that of the node, conduction fails at the transition node, with only a small, rapidly decrementing signal seen. This simulation was very sensitive to the degree of extracellular covering near the transition point. Conduction succeeded if the model segments covered were 11, 12, 13, 18, 22, 26, and 29. Reduction of the thickness of

the Frankenhaeuser-Hodgkin space from 200 to 100 Å was not sufficient to restore conduction, but increasing the internodal Na⁺ channel density from 4% to 5% of the nodal density allowed action potentials to traverse the demyelinated region.

Results from another axon from the same 8-d nerve were different (Fig. 7 A). In this case conduction could be demonstrated optically for at least the first 711 μm of the demyelinated region (the axon could not be followed visually beyond this point). In this fiber numerous macrophages were seen close to the transition node (Fig. 7
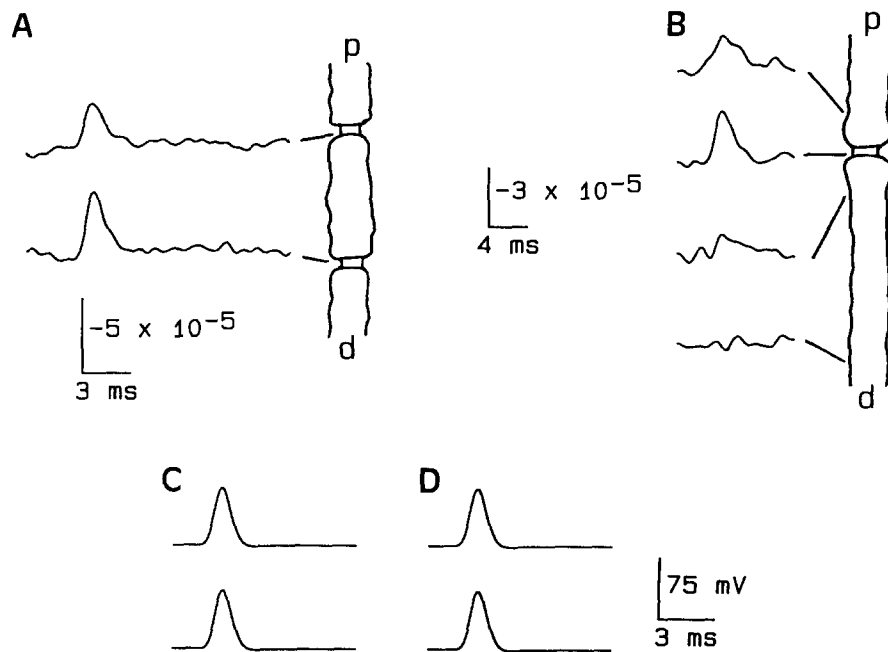

FIGURE 5.   Optical signals from normal nodes of Ranvier. (A) Successive nodes in an uninjected control axon. The internodal distance was 1.5 mm. The fiber diameter, measured across the myelin, was 18 μm. F_c = 0.5 kHz. (B) Optical records at nodal, paranodal, and internodal sites. Measurements at the paranodes were made at a distance of 11 μm from the node. The myelin diameter was 15 μm. F_c = 0.3 kHz. (C) Calculated action potentials from two successive nodes from a model control axon with properties similar to those of the fiber in A. The internodal length was 1.5 mm and the axon diameter was 12 μm, which is within the range seen in fibers with a myelin diameter of 18 μm. The channel densities in the internodal axolemma were set to 4% of those at the nodes. F_c = 0.5 kHz. (D) Calculated action potentials as in C but with the internodal channel density set to zero.

E), and at a more distal area the axolemma was virtually covered with these cells (Fig. 7 F). Conduction through the demyelinated zone was successful, though at a velocity of <1 m/s. We utilized the simulation to explore possible mechanisms for this result. The Na⁺ channel density in the internodal axolemma was set first to 4% of the nodal value. The associated macrophages were modeled as a single-cell layer loosely attached to several sites near the transition node and also further along the demyelinated segment. The distance between the axolemma and the innermost

macrophage membrane was again taken to be 200 Å. With eight sites covered along the internode conduction was successful with a velocity of 1.1. m/s, close to the experimental value (Fig. 7 *B*). Eliminating the internodal Na$^+$ channels resulted in a failure of conduction (Fig. 7 *C*). Varying the density of these channels showed that block occurred with a reduction to <2% of the nodal density. If four of the eight
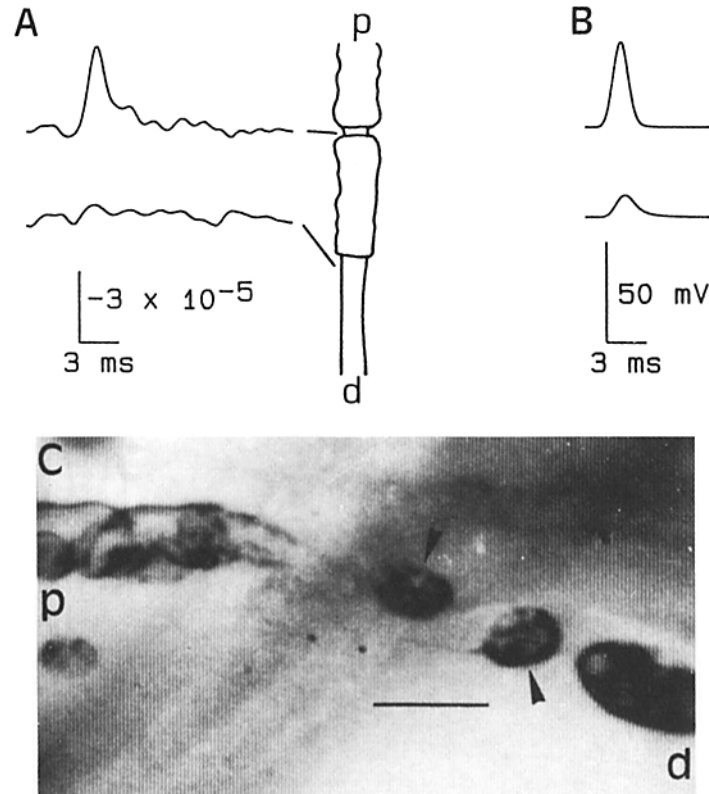

FIGURE 6.   Failure of conduction at the proximal end of a demyelinated zone 8 d after injection. (*A*) Optical records from the last intact proximal node and from the beginning of the demyelinated region, 1.7 mm away. F_c = 0.3 kHz. (*B*) Model calculations for an axon simulating this fiber. Axon diameter, 10 μm. Internodal length, 1.7 mm. Action potentials at the same sites as in *A*, F_c = 0.3 kHz. Internodal channel densities, 4% of nodal values. Internodal axolemma covered by one cell layer at segments 12, 14, 18, 22, 26, and 29. (*C*) Light micrograph of the proximal end of the demyelinated zone of the axon of *A*. Macrophages are bound to the axolemma at scattered sites (*arrow*). Bar, 30 μm.

covered sites were left bare, propagation again was terminated at the transition node (Fig. 7 *D*). Thus, as in the previous case, the model suggests that successful conduction at a transition node depends on a delicate balance among several parameters. For a given internodal Na$^+$ channel density and fiber geometry conduction is most sensitive to the degree of extracellular covering, particularly in the neighborhood of the transition point.
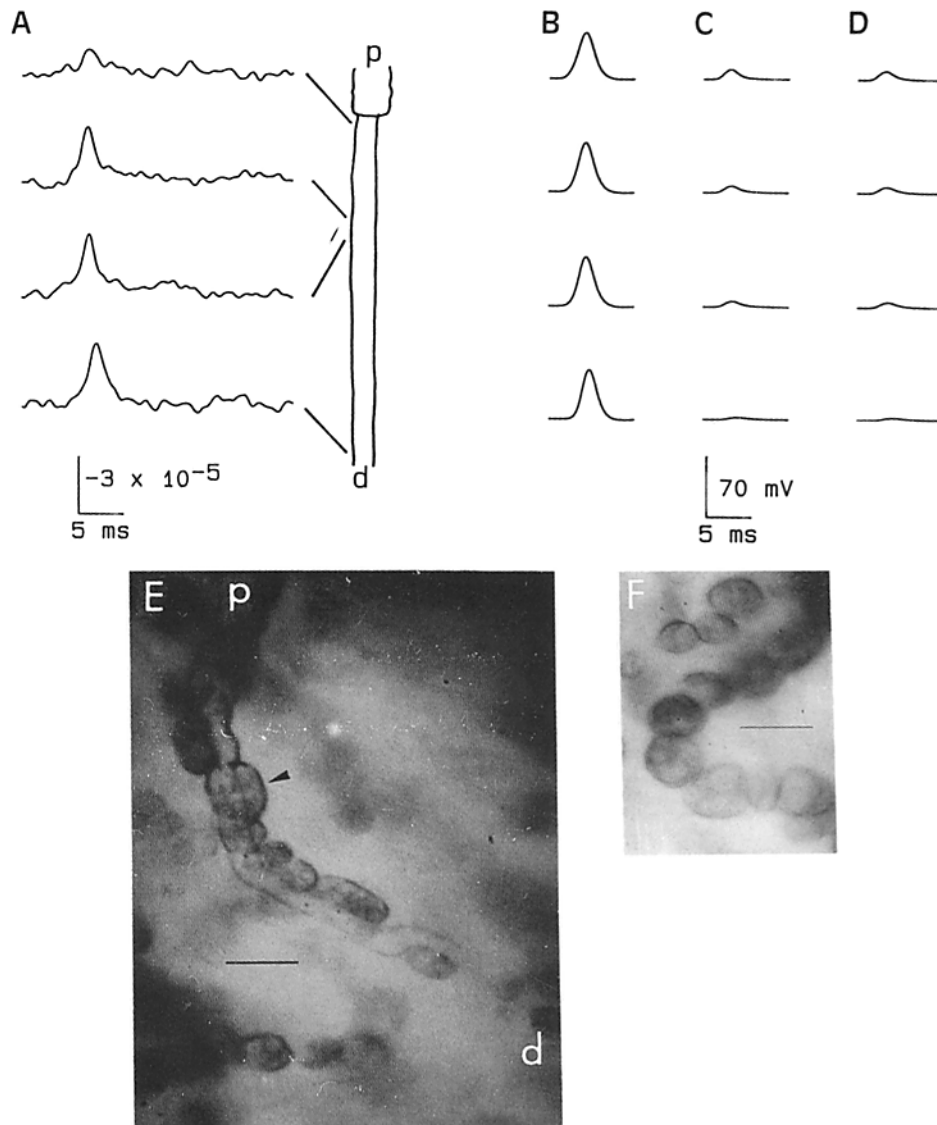
FIGURE 7. Successful continuous conduction along the first 0.7 mm of a demyelinated internode, 8 d after injection. (A) Optical records taken at 0, 203, 254, and 711 μm from the end of myelin. F_c = 0.22 kHz. (B) Calculated action potentials for an axon simulating this fiber. Records at 0, 189, 264, and 714 μm from the proximal end of the demyelinated zone. Axon diameter, 8 μm. Internodal length set to 1.5 mm (typical of fibers of this caliber). Internodal channel densities 4% of the nodal values. Axolemma covered by a single cell layer at segments 12, 13, 15, 16, 18, 22, 26, and 29. F_c = 0.22 kHz. (C) Same, but with internodal channel densities set to zero. (D) Calculated signals as in B, but with the single cell layer only on segments 12, 16, 22, and 29. (E) Light micrograph of the proximal end of the demyelinated zone, showing clusters of macrophages (arrow). (F) Light micrograph of a more distal site along the same demyelinated fiber, with the axon covered by numerous macrophages. Bars, 30 μm.

In some cases small tracts of axons with a common morphology were followed optically at low magnification. Fig. 8 *A* illustrates results from a group of several fibers 6 d after injection. Beginning at the proximal end of the lesion and continuing for ~1 mm these axons appeared completely demyelinated with a large number of bound macrophages. For the next 1.6 mm many axons were surrounded by a loose covering of damaged myelin. This could be judged by the smooth appearance of the myelin, with occasional breaks (Shrager, 1985), and its heavy staining by the dye, indicating an accessibility to individual lamellae that is normally absent. The graph in Fig. 8 *B* plots propagation times vs. distance for these records. The conduc-
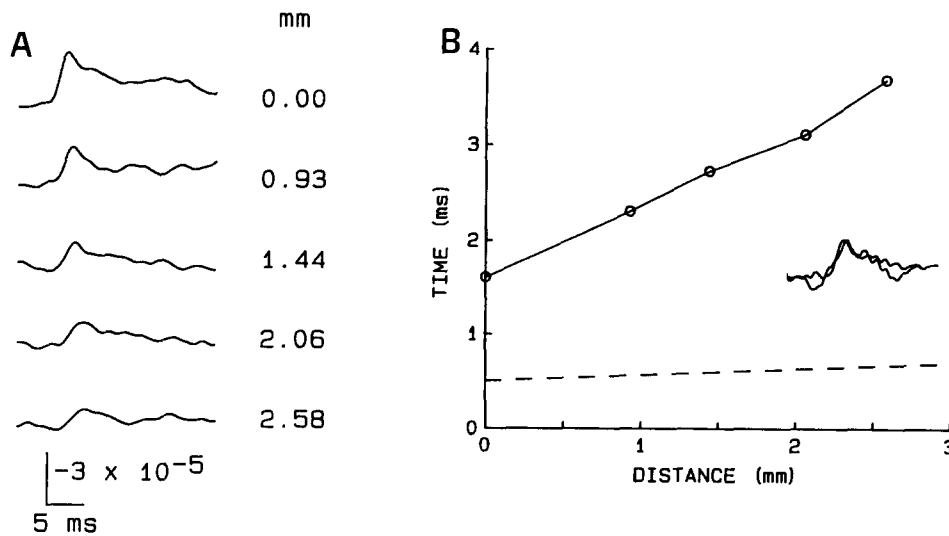

FIGURE 8. Conduction through a small group of uniformly demyelinated axons, 6 d after surgery. The distance covered, 2.58 mm, is greater than the longest internodal length seen in *Xenopus* sciatic nerves (2.2 mm) and is about twice the average internodal length. (*A*) Optical records at low magnification (×10 objective, photodiode field, 40 × 40 μm) at five successive sites, with the most proximal site taken as the origin. F_c = 0.2 kHz. (*B*) Propagation time (time to 50% peak) plotted vs. distance for the records of *A*. The average conduction velocity is 1.3 m/s. The dashed line gives the result that would be expected for uniform conduction in a normal axon of 15 m/s. (*Inset*) The sweeps at 0 and 2.58 mm in *A* redrawn with the traces offset in time so that the rising phases superimpose. F_c = 0.35 kHz.

tion velocity (inverse slope) was relatively constant along this tract, over a distance corresponding to almost two typical internodal lengths, with an average value of 1.3 m/s. In the inset the sweeps at 0 and 2.58 mm have been scaled and offset in time so that the peaks correspond. The signal shapes largely superimpose, as would be expected for propagation at constant velocity. Thus, once begun, action potentials are capable of propagation along considerable lengths of demyelinated axons.

At 8 d after injection, before the appearance of proliferating Schwann cells, optical signals at the first node distal to a long (>1 mm) demyelinated zone were almost never seen. This is reflected in the very small contribution of slowly conducting fibers to the compound action potential at this time (Fig. 4). By 15 days after
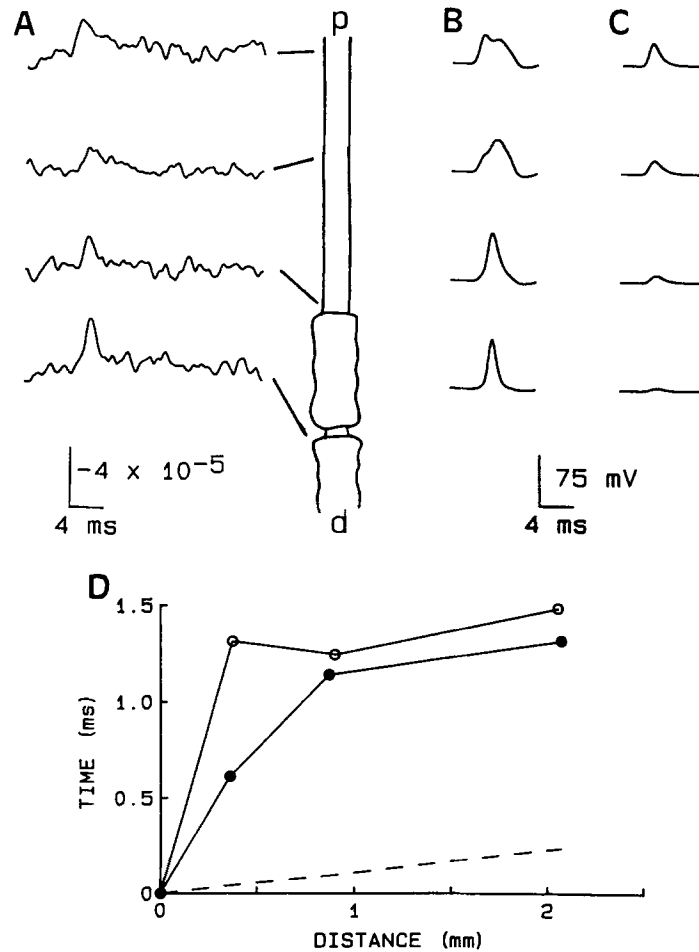
FIGURE 9. Signal propagation completely across an internode in the earliest stages of remyelination, 15 d after injection. (A) Optical sweeps at three sites along the internode and at the first node of Ranvier distal to the remyelinated zone. Distances from the most proximal site (uppermost sweep) were 0, 0.38, 0.90, and 2.1 mm. F_c = 0.5 kHz. (B) Predictions of the model for this axon. Calculated action potentials at 0, 0.36, 0.90, and 2.1 mm. Axon diameter, 4 μm. Internodal length, 1.2 mm. Internodal channel densities, 4% of nodal values. Demyelinated internode covered by two lamellae of new myelin (with no paranodal seals). (C) Calculations as for the model of B but with the internodal channel densities set to zero. Conduction failed if the internodal Na^+ channel density was <1% of the nodal value. (D) Conduction time plotted vs. distance for the optical data (O) and the model of B (●). The conduction time at 0 mm has been set to 0 ms for both cases. The dashed line represents the model prediction for a normal myelinated axon of this caliber.

surgery many axons are wrapped by several turns of new, loosely wound myelin (Fig. 2 D). At this stage we have been able to characterize conduction in single fibers completely through the lesion. In Fig. 9 A optical records are shown for three sites within a demyelinated internode, and also the signal recorded at the first node distal

to this region. Action potentials are widened significantly in time in the internode, but narrow to a normal time course by the first distal node. The model reproduces this behavior for a fiber of similar geometry (Fig. 9 *B*). The calculations were done for an internode with two myelin lamellae and an internodal Na^+ channel density 4% that at the node. Note that, for this early stage of remyelination, we assume that paranodal seals between Schwann cells and the axolemma have not yet formed. In this case, the internodal channels may still play an important role in conduction since eliminating them from the model resulted in conduction failure (Fig. 9 *C*). With three or more lamellae of new myelin, conduction in this simulated axon was successful with no internodal Na^+ channels. The graph in Fig. 9 *D* illustrates conduction times measured both experimentally (O) and from calculated action potentials (●). The experimental points illustrate very slow conduction in the demyelinated internode, and almost normal conduction in the distal myelinated segment (compare to the dashed line, which is calculated for a normal myelinated axon of this geometry). The model reproduces the optical data reasonably well. The differ-
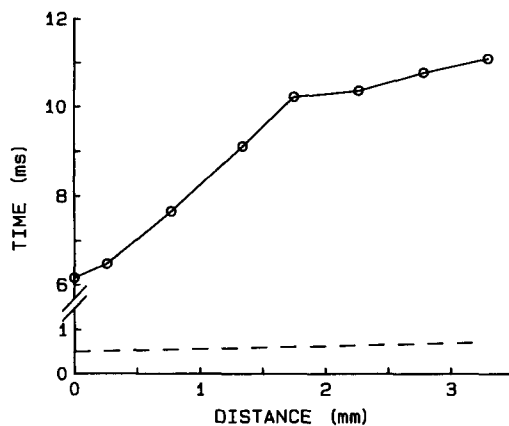

FIGURE 10. Conduction through a tract of a few demyelinated/remyelinating fibers, 15 d after surgery, as measured from optical signals at low magnification (×10 objective, photodiode field 40 × 40 μm). Propagation time is plotted vs. distance over a 3.3-mm span (more than twice the average internodal length). The dashed line represents fibers conducting at 15 m/s. $F_c = 0.5$ kHz.

ence at 0.3 mm may be due to noise resulting from the small size of the optical signal at this site.

Fig. 10 summarizes data for a small group of fibers recorded optically at lower magnification, again at 15 d. The conduction velocity varied from 0.4 m/s at the proximal end of the tract to 1.6 m/s toward the more distal region. This group of axons was excised at the conclusion of the experiment and fixed for electron microscopy. One remyelinating axon within the tract is shown in Fig. 2 *D*.

At 36 d after surgery remyelination has progressed to the point at which new nodes of Ranvier are clearly seen. Internodal distances are typically very short as several new nodes form within each demyelinated internode. In Fig. 11 we show optical records from two successive new nodes, 0.3 mm apart. These signals are among the largest recorded in these studies due partially to the fact that these new nodes are wider than normal, with a correspondingly longer length of exposed axolemma. The conduction velocity measured from these traces is 2.0 m/s, still about an order of magnitude slower than that across a normal internode, even after 5 wk of recovery. The compound action potential shown as the lowest sweep in Fig. 11

has two prominent peaks, with the faster representing normal axons. The second peak, absent in control, uninjected nerve, corresponds in time to the optical records, and thus represents remyelinating axons. The measured difference in arrival times of the two peaks is 1.4 ms, within the 1–1.5-ms delay expected for signals to traverse a 2–3-mm lesion, propagating at 2 m/s.

DISCUSSION

The results of this work show that, whereas conduction does not in general progress beyond the transition point from a normal myelinated region to a completely demyelinated internode, very little glial cell association may be sufficient to restore successful propagation. In fact, the macrophages and Schwann cells that are actively removing damaged myelin by phagocytosis may, if present in sufficient number, provide improvement in the cable properties of the demyelinated zone adequate to enable conduction. We conclude from our optical measurements that the continuous conduction first described by Bostock and Sears (1978) can in fact occur in very long segments of demyelinated nerve, but is very rare before significant ensheath-
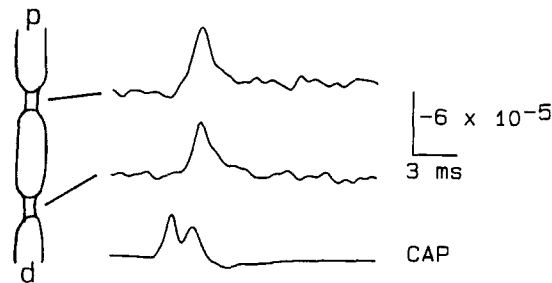

FIGURE 11. Action potentials in new nodes of Ranvier formed during remyelination, 36 d after injection. The top trace is an optical signal from a new node in a remyelinating axon. The middle sweep is the optical record from the next new node distal to the above, 293 μm away. The bottom trace is the compound action potential recorded electrically. The vertical scale applies to both optical records. The time scale is for all three sweeps. $F_c = 0.5$ kHz.

ment by proliferating Schwann cells. Successful bridging of the transition point may occur only in those axons with an extracellular layer at the most proximal region of the demyelinated internode. Alternatively, although each demyelinated zone was normally bordered by former nodes of Ranvier, in occasional axons length measurements indicated that a break in myelin began within an internode. The remaining myelin on the proximal side could then provide sufficient insulation to allow conduction. Calculations with the computational model showed that conduction through a transition point was highly sensitive to the length of the immediately preceding myelinated zone. However, the gradual recruitment of conducting axons during the period of 6–12 d could not be due to changes in this length since, if anything, myelin removal is still proceeding in some fibers during this time. Finally, from recordings of compound action potentials Smith and Hall (1980) found small components with slow velocities at about the time that Schwann cells appeared and before significant remyelination.

The major advantage of the present study is that it has allowed measurements to be made on observable single fibers. Experimental demyelination invariably results

in a heterogeneous population of axons within the cord. The spatial extent of demyelination in an individual axon can range from just a few tens of micrometers to the entire length of the lesioned area (2–3 mm). This is true even for the lysolecithin lesion, in which the temporal progression of events is remarkably constant among different fibers. Signals found to traverse the injected zone in compound action potentials could, in principle, arise from axons with only a very limited extent of demyelination. Thus, it is very difficult to extract physiological information from studies of intact bundles. The significance of the present approach is that it allows measurements to be made on single cells or small tracts that can be characterized visually over a considerable length. One disadvantage of the optical method is that, although it provides information on shape and timing of action potentials, it gives no data on the absolute level of voltage, and allows conclusions about relative amplitudes only in cases in which dye binding and the axolemmal surface area sampled are constant.

We have tested many of our conclusions through the use of a detailed computational model of conduction. A number of studies involving calculations of action potentials in myelinated and demyelinated axons have been published previously (Goldman and Albus, 1968; Koles and Rasminsky, 1972; Waxman and Brill, 1978). Most earlier models assumed that the internodes contained no Na^+ channels, and also considered myelin and axolemma as one parallel resistor-capacitor branch, ignoring the axial pathway in the Frankenhaeuser-Hodgkin space. The system used in this report makes use of the recent experimental measurement of Na^+ channel distributions in demyelinated axons (Shrager, 1987, 1988; Chiu and Schwarz, 1987). We include also ultrastructural data regarding extent and geometry of the extracellular layer present during both the period of progressive removal of myelin and during early remyelination. Finally, we are able to compare calculated signal shapes and conduction times with those determined through optical measurements. The model contains a large number of parameters, but most were placed under tight constraints. The channel properties were those determined for *Xenopus* nerve fibers by Frankenhaeuser and Huxley (1964) and many of the geometrical values came directly from light and electron microscopy. The major uncertainties concerned the conductance of Schwann cell and myelin membranes, and the paranodal seals between myelin and axolemma in the normal regions of the fiber. The former was given a value similar to that of most cell surface membranes. The seals were considered effectively to close this pathway to appreciable current. Alternatively, it has been suggested that much of the unusually high nodal leakage conductance measured in gap-clamp experiments actually results from a distributed pathway through axolemma and Schwann cell in the paranode (Barrett and Barrett, 1982; Baker et al., 1987). Lacking direct experimental evidence on this point, we have retained the classical lumped nodal leak. In the demyelinated zone, the seals were assumed to be absent, and the axial resistance was calculated directly from the geometry and the known resistivity of the extracellular medium. One other parameter that has some uncertainty is the K^+ channel density in the internode. We kept the $Na^+/K^+/P$ channel ratios in the internode identical to those at the nodes. In most of our loose patch clamp experiments we used K^+ channel blockers to improve the accuracy of peak Na^+ current measurements. In the few instances in which these

compounds were absent the results suggested that the K^+/Na^+ channel ratio is somewhat higher in the internodes than in the nodes. In some calculations we set this ratio to 3 in the internodal axolemma, without significant effect on the results. It should, however, be noted that there is now considerable evidence for the existence of several K^+ channel types in myelinated nerve (Dubois, 1981; Baker et al., 1987; Gordon et al., 1988). We are currently attempting to measure K^+ currents and their drug sensitivity in patch clamp experiments. Despite these remaining uncertainties, this model would seem to represent an improvement over earlier versions since it incorporates a number of recent experimental measurements, and since it can be matched at least partially to the cells under examination. The fit to the optical data was in most cases reasonably good.

In running the model under a variety of conditions, some results emerge quite clearly. With an internodal Na^+ channel density of the order determined in experiments, conduction depends critically on the conditions at the transition point from myelinated to demyelinated axon. Very small changes in the extracellular impedance, as by adding or subtracting a single cellular layer over short segments, can change the result from complete block to successful continuous conduction through the entire demyelinated internode. Furthermore, both experiment and theory show that the earliest stages of remyelination greatly improve the probability of success at the transition point, but increase conduction velocity through the demyelinated region only slightly. This is due to the fact that as the number of myelin lamellae increases from zero to about four, the cable properties improve steadily, but the fractional activation of internodal Na^+ channels declines, ultimately reaching zero. The optically measured conduction velocities in the demyelinated/remyelinating internode were in the range of 0.5–1.5 m/s throughout the period of 6–15 d after surgery. These results are reflected in the compound action potential records, which show only a modest improvement in speed, but a strong increase in amplitude over the same time. At 6–8 d after injection, the associated cells (primarily macrophages) do not fully surround the axon. The computational model was radially symmetric to facilitate calculations. However, calculating R_{FH} vs. R_m for patches of cells with separations of 100–200 Å from the axolemma shows that they are of comparable order. Thus, these cells can provide the small improvement required for conduction even without enclosing the fiber, though this may require a cluster of several such cells, as was seen in the fiber of Fig. 7.

In earlier experiments we demonstrated that the internodal Na^+ channels can be activated by a propagating depolarization invading a demyelinated segment (Shrager, 1988). In the present study we show that conduction through these segments may take place at constant velocity, suggesting that these channels play an essential role. We have previously provided evidence from patch clamp measurements, on the one hand, that the density of Na^+ channels in the paranodal axolemma may increase about 2.5-fold during the first week after surgery (Shrager, 1987). The internodal Na^+ channel density did not change significantly, suggesting that there was no large-scale synthesis and insertion of Na^+ channels in response to the demyelination. Thus, the increase in paranodal channels may arise from lateral diffusion from the node. On the other hand, the patch clamp experiments show that the sharp gradient in Na^+ channel density at the node of Ranvier persists for several

months after demyelination, indicating that only a fraction of the nodal channels may be mobile (Shrager, 1988, 1989). However, when we constructed the model so that 50% of the nodal channels were distributed uniformly over 17 μm of the paranode (a 2.5-fold increase in paranodal Na^+ channel density), conduction still failed at the proximal demyelinated node (segment 10). In this test no macrophages or Schwann cells were considered attached to the axolemma. Thus, the model predicts that Na^+ channel spread alone may be insufficient for restoration of conduction. More extensive calculations are in progress to see if a combination of lateral diffusion and early Schwann cell binding are more effective than either alone.

Our results suggest that very small improvements in passive cable properties at transition sites effected by the close association of glial or other cells, may suffice to restore conduction in compromised fibers. In the peripheral nervous system, Schwann cells proliferate rapidly after demyelination and remyelinate affected axons. Continuous conduction through demyelinated regions is thus a transient phenomenon, normally superceded by early remyelination, though it may hasten functional recovery. In the central nervous system, in contrast, oligodendrocytes divide with much less frequency and remyelination is relatively rare, and is often incomplete (Raine, 1978). Our loose patch clamp experiments and the gap-clamp results of Chiu and Schwarz (1987) have shown that the internodal axolemma of mammalian axons has a density of Na^+ channels similar to that of amphibian fibers. In multiple sclerosis, a demyelinating disease of the central nervous system, patients often remit spontaneously with significant return of function after an acute paralytic episode, despite the apparent lack of remyelination. Although one must be careful in extending results on peripheral axons to the central nervous system, the experiments presented here suggest a mechanism that may contribute to this restoration of conduction.

REFERENCES

Baker, M., H. Bostock, P. Grafe, and P. Martius. 1987. Function and distribution of three types of rectifying channel in rat spinal root myelinated axons. *Journal of Physiology.* 383:45–67.

Barrett, E. F., and J. N. Barrett. 1982. Intracellular recordings from vertebrate myelinated axons: mechanisms of the depolarizing after-potential. *Journal of Physiology.* 323:117–144.

Bostock, H., and T. A. Sears. 1978. The internodal axon membrane: electrical excitability and continuous conduction in segmental demyelination. *Journal of Physiology.* 280:273–301.

Chiu, S. Y., and W. Schwarz. 1987. Sodium and potassium currents in acutely demyelinated internodes of rabbit sciatic nerves. *Journal of Physiology.* 391:631–649.

Cohen, L. B., and S. Lesher. 1986. Optical monitoring of membrane potential: Methods of multi-

site optical measurement. *In* Optical Methods in Cell Physiology. P. DeWeer and B. M. Salzberg, editors. Wiley-Interscience, New York. 71–99.

Cohen, L. B., and B. M. Salzberg. 1978. Optical measurement of membrane potential. *Reviews of Physiology, Biochemistry, and Pharmacology.* 83:35–88.

Colquhoun, D., and F. J. Sigworth. 1983. Fitting and statistical analysis of single-channel records. *In* Single Channel Recording. B. Sakmann and E. Neher, editors. Plenum Press, New York. 191–263.

Dubois, J. M. 1981. Evidence for the existence of three types of potassium channels in the frog Ranvier node membrane. *Journal of Physiology.* 318:297–316.

Frankenhaeuser, B., and A. L. Hodgkin. 1956. The after-effects of impulses in the giant nerve fibres of *Loligo. Journal of Physiology.* 131:341–376.

Frankenhaeuser, B., and A. F. Huxley. 1964. The action potential in the myelinated nerve fibre of *Xenopus laevis* as computed on the basis of voltage clamp data. *Journal of Physiology.* 171:302–315.

Goldman, L., and J. S. Albus. 1968. Computation of impulse conduction in myelinated fibers: theoretical basis of the velocity-diameter relation. *Biophysical Journal.* 8:596–607.

Gordon, T. R., J. D. Kocsis, and S. G. Waxman. 1988. Evidence for the presence of two types of potassium channels in rat optic nerve. *Brain Research.* 447:1–9.

Grinvald, A. 1985. Real-time optical mapping of neuronal activity: From growth cones to the intact mammalian brain. *Annual Reviews of Neuroscience.* 8:263–305.

Grinvald, A., W. N. Ross, and I. C. Farber. 1981. Simultaneous optical measurements of electrical activity from multiple sites on processes of cultured neurons. *Proceedings of the National Academy of Sciences.* 78:3245–3249.

Hall, S. M., and N. A. Gregson. 1971. The in vivo and ultrastructural effects of injection of lyso-phosphatidyl choline into myelinated peripheral nerve fibers of the adult mouse. *Journal of Cell Science.* 9:769–789.

Hille, B. 1971. The permeability of the sodium channel to organic cations in myelinated nerve. *Journal of General Physiology.* 58:599–619.

Hines, M. 1989. A program for simulation of nerve equations with branching geometries. *International Journal of Biomedical Computing.* 24:55–68.

Koles, Z. J., and M. Rasminsky. 1972. A computer simulation of conduction in demyelinated nerve fibres. *Journal of Physiology.* 227:351–364.

Lev-Ram, V. and A. Grinvald. 1986. Ca^{++} and K^+-dependent communication between central nervous system myelinated axons and oligodendrocytes revealed by voltage-sensitive dyes. *Proceedings of the National Academy of Sciences.* 83:6651–6655.

Lev-Ram, V., and A. Grinvald. 1987. Early demyelination can be detected in vitro by a myelin associated optical signal. *Journal of Neuroimmunology.* 16:106. (Abstr.)

Milton, R. L., R. T. Mathias, and R. S. Eisenberg. 1985. Electrical properties of the myotendon region of frog twitch muscle fibers measured in the frequency domain. *Biophysical Journal.* 48:253–267.

Raine, C. S. 1978. Pathology of demyelination. *In* Physiology and Pathobiology of Axons. S. G. Waxman, editor. Raven Press, New York. 282–311.

Ritchie, J. M., and R. B. Rogart. 1977. The density of sodium channels in mammalian myelinated nerve fibers and the nature of the axonal membrane under the myelin sheath. *Proceedings of the National Academy of Sciences.* 74:211–215.

Rubinstein, C., and P. Shrager. 1989. Optical recording of action potentials in demyelinated and remyelinating frog nerve fibres. *Journal of Physiology.* 418:18P. (Abstr.)

Shrager, P. 1987. The distribution of sodium and potassium channels in single demyelinated axons of the frog. *Journal of Physiology.* 392:587–602.

Shrager, P. 1988. Ionic channels and signal conduction in single remyelinating frog nerve fibres. *Journal of Physiology.* 404:695–712.

Shrager, P. 1989. Sodium channels in single demyelinated mammalian axons. *Brain Research.* 483:149–154.

Shrager, P., S. Y. Chiu, J. M. Ritchie, D. Zecevic, and L. B. Cohen. 1987. Optical recording of action potential propagation in demyelinated frog nerve. *Biophysical Journal.* 51:351–355.

Shrager, P., C. Rubinstein, and E. Brunschweiger. 1989. Conduction measured in single demyelinated and remyelinating axons using optical techniques. *Abstracts of the Society for Neuroscience.* 15:538.

Smith, K. J., and S. M. Hall. 1980. Nerve conduction during peripheral demyelination and remyelination. *Journal of the Neurological Sciences.* 48:201–219.

Stampfli, R. 1952. Bau und Funktion isolierter markhaltiger Nervenfasern. *Ergebnisse der Physiologie.* 47:70–165.

Waxman, S. G. and M. H. Brill. 1978. Conduction through demyelinated plaques in multiple sclerosis: computer simulations of facilitation by short internodes. *Journal of Neurology, Neurosurgery, and Psychiatry.* 41:408–417.